Element Efficiency and Noise in Grid Arrays

Michael P. De Lisio, *Member, IEEE,* Robert M. Weikle II, *Member, IEEE,* and David B. Rutledge, *Fellow, IEEE*

(Invited Paper)

Abstract—The element efficiency of a phased array is the ratio of the radiated-to-available power of a single element, when only that element is excited. We relate this element efficiency to the output noise power generated by a quasi-optical grid amplifier array. Both electromagnetic and thermodynamic derivations will be presented. These ideas will be used to predict the total noise power and noise radiation pattern of grid arrays. The results are also extended to show that the output noise temperature of the entire array will be the same as the output noise temperature of a single element.

Index Terms— Element efficiency, grid arrays, noise, quasi-optics.

I. INTRODUCTION

QUASI-OPTICS has attracted increasing attention. By combining the outputs of many solid-state devices in air, high output powers are possible. Furthermore, the planar nature of quasi-optical components makes them amenable to conventional semiconductor fabrication and mass production. Quasi-optical amplifiers have shown considerable promise. Measurements of grid [1], [2] and array [3] amplifiers have shown that the entire array noise does not increase with the number of devices incorporated. The signal power, on the other hand, does increase with the number of elements. This important result implies that the dynamic range of quasi-optical amplifier will increase with the number of devices.

In this paper, we present a theoretical study of the noise properties of quasi-optical amplifier arrays. Our study will concentrate on grid arrays—which tend to have small unit cells—in particular. The approach, however, is general and applies to larger cell amplifier arrays as well. We must stress that our analysis is specific to amplifier arrays. Phase noise in oscillator arrays has been measured [4], [5]. A complete analysis (like Chang and York's [5]) must include the oscillator's complicated nonlinear dynamics. Moreover, Hacker's noise radiation pattern measurements in [4] suggest that the individual phase noise sources are highly correlated.
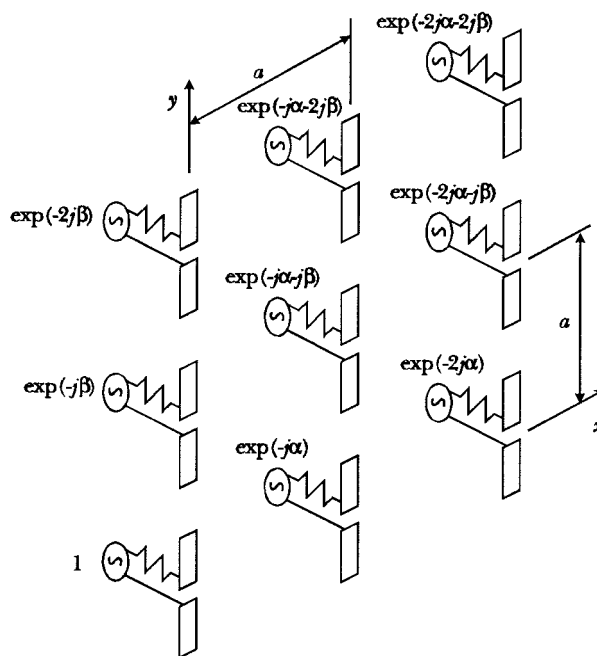
Fig. 1. Section of a large planar phased antenna array.

II. ELEMENT EFFICIENCY

Our approach is based on the radiation efficiency of a single element in an array antenna. This element efficiency relates the power radiated by a single element in an array to the power available to that element, when only the one element is excited. Element efficiency was first proposed by Hannan [6] and later extended by Kahn and Wasylkiwskyj [7], [8] in the study of conventional phased-array antennas. In this section, we will reproduce some of their original derivations for completeness. Further details can be found by referring to the original literature. Pozar [9] has recently explored the active element pattern as well.

Consider a planar rectangular phased antenna array (like the one shown in Fig. 1). When the number of elements in the array is large, the behavior of each element will be nearly identical, except for the few peripheral elements. It is convenient to deduce the properties of this large array by considering an infinite array. The element spacing in both the x- and y-directions is a. In quasi-optical parlance, a is the size of the unit cell. Generators with an internal impedance Z_g excite the elements. All generators have identical magnitudes, but differing phases. The progressive phase delay between adjacent generators is α in the x-direction and β in the
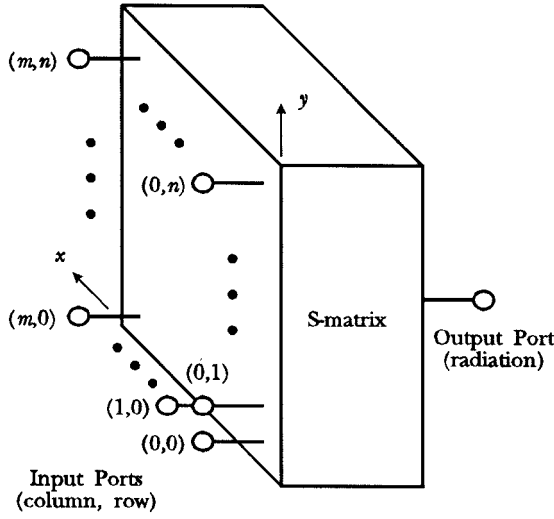
Fig. 2.   Representation of a large planar phased antenna array as a lossless scattering network. The output port represents plane-wave radiation.

y-direction. The main beam of this phased array will have a peak in the scan direction given by

$$\sin\theta\cos\phi = \frac{\alpha\lambda_0}{2\pi a} \tag{1a}$$

$$\sin\theta\sin\phi = \frac{\beta\lambda_0}{2\pi a} \tag{1b}$$

where λ_0 is the free-space wavelength. Phases α and β exist from $-\pi$ to $+\pi$ radians, but the main-beam scan angle will only exist when the relation

$$\left(\frac{\alpha\lambda_0}{2\pi a}\right)^2 + \left(\frac{\beta\lambda_0}{2\pi a}\right)^2 \le 1 \tag{2}$$

is satisfied. For phase delays outside this range, the main beam will not be visible.

Each generator in the array sees the same antenna impedance. This impedance will be a function of the phase delays and is often referred to as the active impedance of the array $Z(\alpha, \beta)$. We also define an active reflection coefficient

$$\rho(\alpha, \beta) = \frac{Z(\alpha, \beta) - Z_g^*}{Z(\alpha, \beta) + Z_g} \tag{3}$$

based on the complex generator impedance Z_g. Note that for phase delays outside the range specified in (2), no main beam is visible and $|\rho(\alpha, \beta)|$ must be unity, implying $Z(\alpha, \beta)$ is purely imaginary.

The antenna array can also be thought of in terms of a lossless scattering network, as shown in Fig. 2. For an infinite array, the scattering parameters will depend only on the relative distance between any two individual elements, not on the absolute element location. We define the scattering parameter s_{mn} as the ratio of the normalized power wave emerging from an element in column m, row n to the normalized power wave incident on an element in column 0, row 0. All input ports should be terminated in the generator impedance Z_g. When only one element is excited with unit

incident power, the radiated power will be given by

$$\eta = 1 - \sum_{m=-\infty}^{\infty}\sum_{n=-\infty}^{\infty}|s_{mn}|^2. \tag{4}$$

This normalized power is the ratio of the power radiated from a single element to the power available to the same element when only that element is excited. This ratio is the definition of the element efficiency η [6].

We are now in a position to relate the element efficiency to the active reflection coefficient. Assume all elements are now excited with proper phasing. Using superposition, we find

$$\rho(\alpha, \beta) = \sum_{m=-\infty}^{\infty}\sum_{n=-\infty}^{\infty}s_{mn}e^{-j\alpha m}e^{-j\beta n}. \tag{5}$$

This Fourier-series relation can be inverted to obtain

$$s_{mn} = \frac{1}{\pi^2}\int_0^{\pi}\int_0^{\pi}\rho(\alpha, \beta)e^{j\alpha m}e^{j\beta n}\,d\alpha\,d\beta \tag{6}$$

exploiting the even parity of $\rho(\alpha, \beta)$ with respect to α and β due to the array's symmetry. Equations (5) and (6) must also obey a Parseval relation

$$\sum_{m=-\infty}^{\infty}\sum_{n=-\infty}^{\infty}|s_{mn}|^2 = \frac{1}{\pi^2}\int_0^{\pi}\int_0^{\pi}|\rho(\alpha, \beta)|^2\,d\alpha\,d\beta. \tag{7}$$

We are now able to express the element efficiency in terms of the active reflection coefficient using (4) and (7)

$$\eta = \frac{1}{\pi^2}\int_0^{\pi}\int_0^{\pi}\left[1 - |\rho(\alpha, \beta)|^2\right]d\alpha\,d\beta. \tag{8}$$

The element efficiency can be interpreted as the radiated-power transmission coefficient averaged over all possible row and column phase delays.

III. THE IDEAL ELEMENT

Hannan [6] and Kahn [7] define an ideal element as one that is matched for all visible main-beam scan angles. For phase delays inside the circular boundary given by (2), $\rho(\alpha, \beta)$ will be zero. For phase delays outside this region, the main beam is not visible and $|\rho(\alpha, \beta)|$ will be unity. When the element spacing a is less than $\lambda_0/2$, the ideal efficiency η_i will be

$$\eta_i = \frac{\pi a^2}{\lambda_0^2} = \frac{\pi A_{\text{cell}}}{\lambda_0^2} \tag{9}$$

where A_{cell} is the area of the unit cell. This is the most important result for grid arrays, which tend to have rather small unit-cell sizes. For element spacings between $\lambda_0/2$ and $\lambda_0/\sqrt{2}$, (8) must be integrated directly to find η_i. For element spacings larger than $\lambda_0/\sqrt{2}$, η_i will be unity. When the element spacing is greater than $\lambda_0/2$, one must also be careful to avoid the excitation of grating lobes; usually the element pattern is truncated to suppress their appearance. Fig. 3 shows the ideal element efficiency for an infinite square array with element spacing (unit cell size) a.
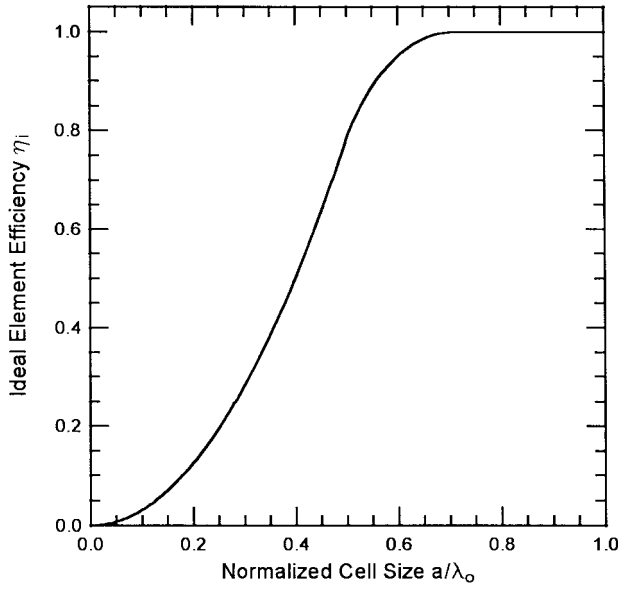
Fig. 3. Ideal element efficiency η_i for an infinite planar array. The unit cell is square with dimension a on a side.

Using an argument based on physical intuition, Hannan [6] concludes that the realized antenna gain of a single excited element $g_r(\theta, \phi)$ must be

$$g_r(\theta, \phi) = \frac{4\pi A_{\text{cell}}}{\lambda_0^2} \cos\theta \left[1 - |\rho(\alpha, \beta)|^2\right]. \quad (10)$$

Equation (10) is a true antenna gain—it is based on the power available to the element. We see that the element pattern of an ideal element will be proportional to $\cos\theta$. However, if grating lobes can exist, this ideal pattern must be truncated to avoid their excitation. For nonideal elements, $|\rho(\alpha, \beta)|$ will not necessarily be zero. If, however, the nonideal array is matched for a normal beam, the element pattern will be somewhat narrower than $\cos\theta$.

IV. A Thermodynamic Approach

The preceding results are based entirely on the arguments presented in [6]–[8]. These results can be explained quite naturally in thermodynamic terms as well. We first consider a large array of N closely spaced ($a \leq \lambda_0/2$) ideal elements. We will consider nonideal elements later. The array is placed on a ground plane such that it only radiates into a hemisphere. Each element is excited by a noisy matched load with noise temperature T. The noise power in a unit bandwidth available to any element is simply kT, where k is Boltzman's constant. Each ideal element radiates a noise power spectral density of $\eta_i kT$, where η_i is the ideal element efficiency defined in Section III. Assuming all the noise sources are uncorrelated, the total noise power spectral density radiated by the N elements in the array P_r will be

$$P_r = N\eta_i kT. \quad (11)$$

Next, we note that this array of ideal elements is, by definition, matched for all possible angles of the main beam. The reciprocal relation must also hold: the array must not reflect plane waves incident from any angle. In this way, the entire array resembles an ideal blackbody. The power spectral density per unit solid angle radiated by this blackbody is defined as the radiation intensity $U_n(\theta, \phi)$. The radiation intensity can be obtained from the Rayleigh–Jeans brightness law, valid for low frequencies where quantum effects can be neglected, as follows:

$$U_n(\theta, \phi) = \frac{kT}{\lambda_0^2} A_{\text{array}} \cos\theta \quad (12)$$

where A_{array} is the area of the entire array. Note that A_{array} is simply $N A_{\text{cell}}$. Furthermore, (12) is derived assuming the radiated power is in a single polarization. The total power per unit bandwidth radiated by the blackbody is obtained by integrating (12) over a hemisphere

$$P_r = \int_{\theta=0}^{\pi/2} \int_{\phi=0}^{2\pi} U_n(\theta, \phi) \sin\theta \, d\theta \, d\phi = \pi \frac{kT}{\lambda_0^2} N A_{\text{cell}} \quad (13)$$

which is the well-known result for a Lambertian source. Equating (13) and (11) gives an expression for η_i identical to (9). We also see immediately from (12) that the ideal element radiation pattern must have a $\cos\theta$ dependence.

For nonideal elements, the realized antenna gain of a single excited element can be deduced from (12) and introduces an emissivity factor $\epsilon(\theta, \phi)$

$$g_r(\theta, \phi) = \frac{4\pi A_{\text{cell}}}{\lambda_0^2} \epsilon(\theta, \phi) \cos\theta. \quad (14)$$

where $\epsilon(\theta, \phi)$ is unity for an ideal blackbody. Like (10), this antenna gain is based on the power available to the element kT. Comparing (14) to (10) allows us to relate the active reflection coefficient to the emissivity in the traditional manner

$$\epsilon(\theta, \phi) = 1 - |\rho(\alpha, \beta)|^2. \quad (15)$$

Equation (1) provides a mapping between the (α, β) and (θ, ϕ) domains. Finally, we write an expression for the total-noise power spectral density radiated by a nonideal array as a solid-angle integral

$$P_r = 4 \frac{kT}{\lambda_0^2} A_{\text{array}} \int_{\theta=0}^{\pi/2} \int_{\phi=0}^{\pi/2} \epsilon(\theta, \phi) \cos\theta \sin\theta \, d\theta \, d\phi. \quad (16)$$

The symmetry of the large planar array demands that the element pattern display a fourfold symmetry dictated by the four quadrants of the azimuth angle ϕ. Noting that the Jacobian J [10] of the mapping from the (α, β) domain to the (θ, ϕ) domain is

$$J = \begin{vmatrix} \dfrac{\partial \alpha}{\partial \theta} & \dfrac{\partial \alpha}{\partial \phi} \\ \dfrac{\partial \beta}{\partial \theta} & \dfrac{\partial \beta}{\partial \phi} \end{vmatrix} = \frac{4\pi^2}{\lambda_0^2} A_{\text{cell}} \cos\theta \sin\theta \quad (17)$$

we can recast (16) to read

$$P_r = NkT \frac{1}{\pi^2} \int_0^\pi \int_0^\pi \left[1 - |\rho(\alpha, \beta)|^2\right] d\alpha \, d\beta. \quad (18)$$

Again, we note that the active reflection coefficient will have unit magnitude for values of α and β corresponding to invisible beam angles. Since kT is the power available to a

single element, (18) predicts an element efficiency η identical to (8).

Of particular interest to the experimenter is the noise power spectral density radiated normal to the array. For quasi-optical grid arrays, it is reasonable to assume that the generator is conjugate matched for normal beam angles. That is, $\rho(\alpha = 0, \beta = 0) = 0$ and $\epsilon(\theta = 0, \phi = 0) = 1$. This assumption has been confirmed experimentally by Kim using a lens-focused network analyzer [1]. Under these conditions, the noise intensity radiated normally from a grid of N uncorrelated sources at temperature T is given by (12) with the angle θ set to zero. This confirms the assumptions made by Kim [1] when first measuring the noise of grid amplifier arrays. Note, (12) holds for both ideal as well as nonideal elements. Nonideal elements radiate less total power than ideal ones, but the normal intensity of the two will be identical due to the narrower nonideal element pattern.

We have shown that the concepts of element efficiency and its effect on element radiation patterns in phased arrays apply quite naturally to noisy quasi-optical arrays. Furthermore, the relevant conclusions can be readily derived using thermodynamic concepts.

V. CALCULATIONS FOR GRID ARRAYS

In this section, we present element efficiency calculations for grid arrays based on the above derivations. Before proceeding, it is necessary to calculate the active impedance of an infinite array $Z(\alpha, \beta)$. We use a modified version of the induced electromotive force (EMF) technique used to analyze grid oscillators [11], [12]. A sample unit cell is shown in Fig. 4. A vertical strip of width w is centered in a unit cell with dimension a. An assumed y-directed surface current distribution $K(x, y)$ is also shown in Fig. 4. The surface current is uniform across the strip width w and most of the strip length a. Within some small distance δ from the cell boundary, the current falls linearly to zero. This current taper is necessary to obtain convergent solutions for the active impedance. The grid is fabricated on the front of a dielectric substrate with a relative dielectric constant ε_r and a thickness t. A perfectly reflecting ground plane is on the rear of the substrate.

To compute the active impedance, we write our assumed surface current as a series

$$K(x, y) = \sum_{m=-\infty}^{\infty} \sum_{n=-\infty}^{\infty} K_{mn} e^{-j\alpha'_m x/a} e^{-j\beta'_n y/a} \qquad (19)$$

where

$$\alpha'_m = \alpha + 2\pi m \qquad (20a)$$
$$\beta'_n = \beta + 2\pi n. \qquad (20b)$$

Equations (20a) and (20b) are necessary to account for the row and column progressive phase delays. Solving (19) for K_{mn} gives

$$K_{mn} = \frac{1}{a^2} \int_0^a \int_0^a K(x, y) e^{j\alpha'_m x/a} e^{j\beta'_n y/a} \, dx \, dy. \qquad (21)$$
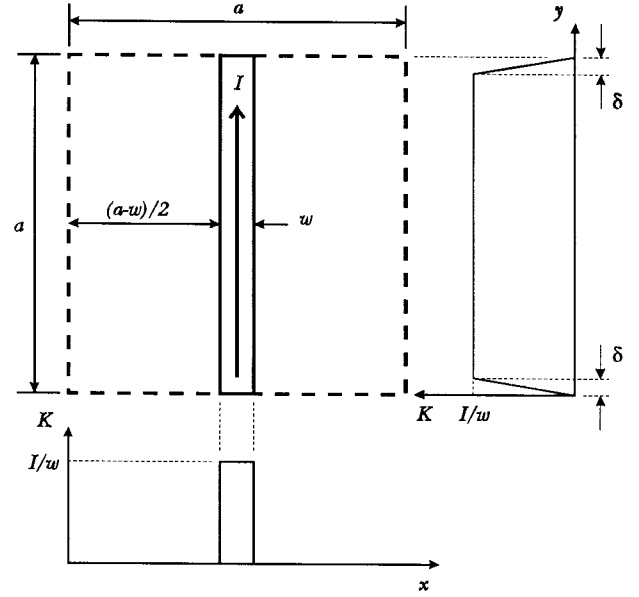

Fig. 4.   Unit cell and assumed surface current $K(x, y)$.

We use the induced EMF technique [11], [12] to find the active impedance

$$Z(\alpha, \beta) = \frac{a^2}{|I|^2} \sum_{m=-\infty}^{\infty} \sum_{n=-\infty}^{\infty} |K_{mn}|^2 Z_{mn}^{\text{eff}}. \qquad (22)$$

I is the total current flowing in the strip. Z_{mn}^{eff} is an effective mode impedance related to the TE and TM-to-z [13] impedances seen by the grid in the $+z$- and $-z$-directions as follows:

$$Z_{mn}^{\text{eff}} = \frac{\alpha'^2_m \left(Z_{\text{TE}mn}^+ \| Z_{\text{TE}mn}^- \right) + \beta'^2_n \left(Z_{\text{TM}mn}^+ \| Z_{\text{TM}mn}^- \right)}{\alpha'^2_m + \beta'^2_n}. \qquad (23)$$

Since we have only estimated the current distribution, the EMF technique will only approximate the active impedance. If more accuracy is required, the current distribution could be refined using the method of moments—an approach that has shown success in analyzing grid arrays [14], [15].

Once the active impedance has been computed, the active reflection coefficient $\rho(\alpha, \beta)$ can be determined from (3). We also assume that the grid is conjugate matched at normal incidence $Z(\alpha = 0, \beta = 0) = Z_g^*$. Equation (8) can then be numerically integrated. The normalized element efficiency η/η_i as a function of cell size is plotted in Fig. 5. For cell sizes less than $\lambda_0/3$, the computed element efficiency is within 80% (1 dB) of its ideal value. The element patterns can also be extracted from the active impedance using (10). Based on the arguments presented in Section IV, the grid's noise will follow the element radiation pattern. Element patterns are shown in Fig. 6 for a cell size of $\lambda_0/4$. Both E- and H-plane patterns are somewhat narrower that the $\cos \theta$ pattern, which accounts for the actual element efficiency only being 83% of the ideal. The E-plane pattern is quite a bit narrower than the H-plane, as expected from the assumed current distribution.
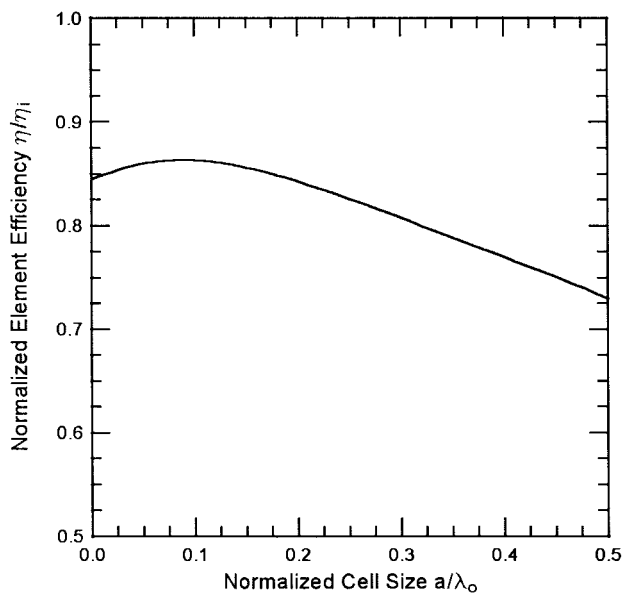
Fig. 5. Normalized element efficiency η/η_i versus cell size a for a grid array. The strip width w is $a/10$ and the substrate is air with a ground plane $\lambda_0/4$ away.
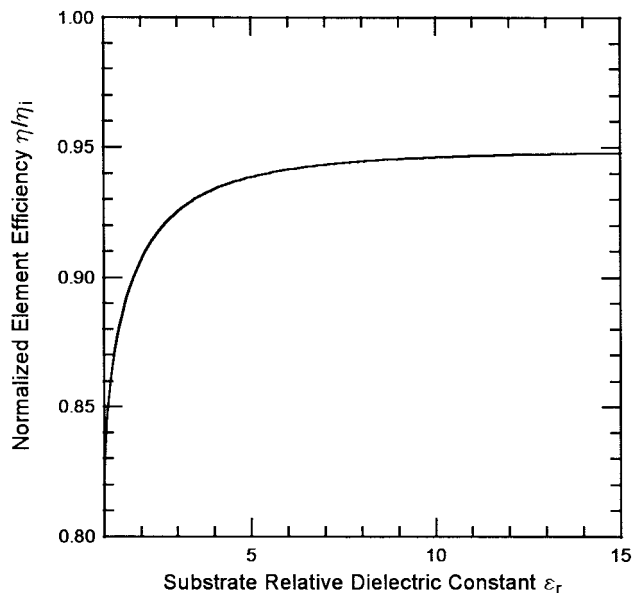

Fig. 7. Normalized element efficiency η/η_i versus substrate dielectric constant ε_r for a grid array. The cell size a is $\lambda_0/4$, strip width w is $a/10$, and the substrate thickness t is $\lambda_0/(\sqrt{\varepsilon_r}4)$.
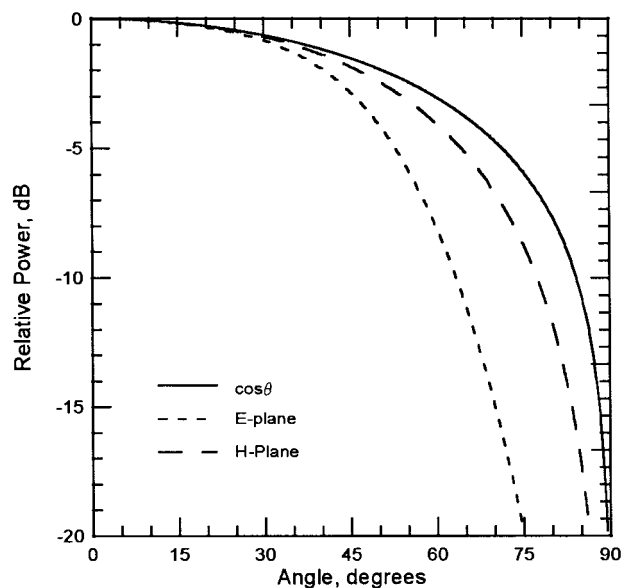

Fig. 6. Relative element patterns for an array with $a = \lambda_0/4$, $w = a/10$, and an air substrate with a ground plane $\lambda_0/4$ away.
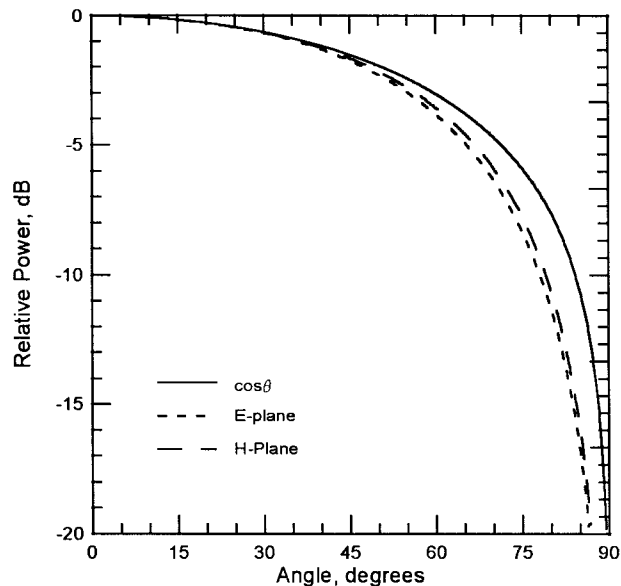

Fig. 8. Relative element patterns for an array with $a = \lambda_0/4$, $w = a/10$, and substrate with $\varepsilon_r = 15$ and thickness $t = \lambda_0/(4\sqrt{15})$.

One reason for the departure from the ideal element efficiency is the active impedance variation with phase angle. Part of this is caused by the mirror behind the array: at nonnormal scan angles, the effective mirror location is closer by a factor of $\cos\theta$. This problem can be alleviated somewhat by placing the grid on a high-dielectric substrate. Even if the scan angle varies considerably, the angle of incidence in the dielectric will not, due to Snell's law. This is verified in Fig. 7. The element efficiency grows with the substrate dielectric constant, with the most rapid growth occurring within $\varepsilon_r = 4$. Fig. 8 plots the element pattern for an array constructed on a substrate with ε_r of 15 and a thickness of a dielectric quarter-wavelength.

Both E- and H-plane patterns are very close to $\cos\theta$, which accounts for the high element efficiency of 95%.

As a final comment, we note that it is possible to compute the element efficiency from an assumed element pattern using (16). For a grid array, it is quite natural to assume the element pattern will be that of a uniform y-directed line current of length a in front of a mirror. We suspect that this approach will not be particularly accurate, however, because it neglects any interaction between elements. Fig. 9 shows a typical element pattern. Since this element pattern is quite different from $\cos\theta$, one would expect a rather low element efficiency. Fig. 10 confirms this suspicion—the element efficiency is only 74% for $a = \lambda_0/4$.
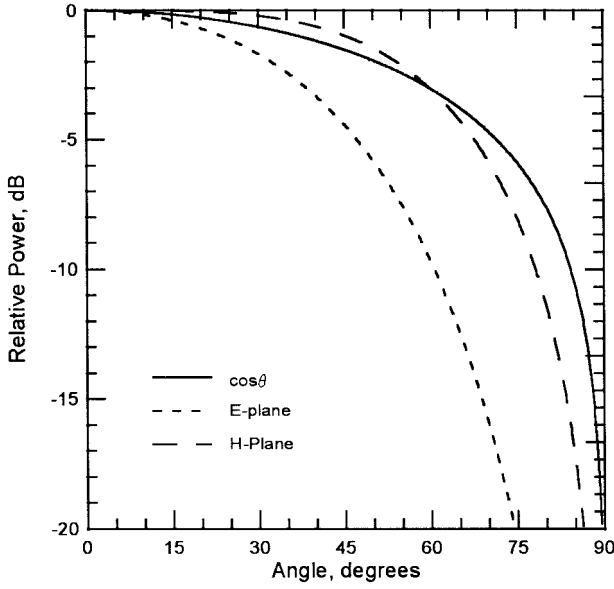
Fig. 9. Assumed element patterns for a line current with length $a = \lambda_0/4$ and an air substrate with a ground plane $\lambda_0/4$ away.
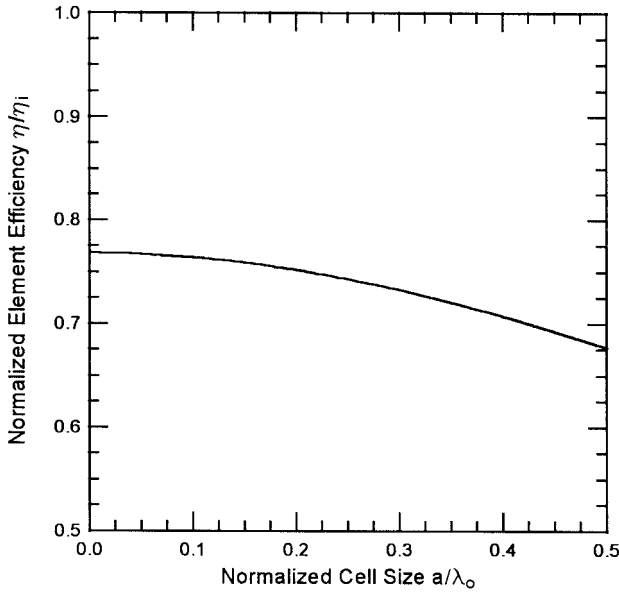

Fig. 10. Normalized element efficiency η/η_i versus cell size a for an element with an assumed line–current pattern. The substrate is air with a ground plane $\lambda_0/4$ away.

VI. SIGNAL-TO-NOISE RATIO

In this section, we investigate the effect of element efficiency on the quasi-optical system's signal-to-noise ratio. We first consider total signal and noise radiated power. In a properly matched grid, the total radiated signal power must be N times the power available from a single element P_0. The total noise power radiated will be given by (13). This gives a signal-to-noise ratio of

$$\frac{P_s}{P_n} = \frac{P_0}{kT\eta} = \frac{P_0}{kT}\frac{\lambda_0^2}{\pi A_{\text{cell}}}\frac{\eta_i}{\eta}. \qquad (24)$$

The results of Section V show that η_i/η will be slightly larger than unity for grid arrays. Equation (24) implies that the total

signal-to-noise ratio will not depend on the number of elements in the array. This conclusion, however, is slightly misleading. The radiated noise power will follow the element pattern, but the signal power pattern will be considerably sharper due to the array factor. The ratio of signal-to-noise intensity radiated normal to the array surface may be a more useful measure. The noise intensity $U_n(0, 0)$ is given by (12) and the signal radiated intensity will be

$$U_s(0, 0) = NP_0\frac{A_{\text{array}}}{\lambda_0^2} = P_s\frac{A_{\text{array}}}{\lambda_0^2}. \qquad (25)$$

This leads to a signal-to-noise normal intensity ratio of

$$\frac{U_s(0, 0)}{U_n(0, 0)} = N\frac{P_0}{kT} = \frac{P_s}{kT}. \qquad (26)$$

This result can be interpreted in two ways. For a given output power per device, the output signal-to-noise ratio measured by an antenna along the optical axis of a grid array will, in fact, grow with the total number of devices incorporated. Another interpretation is for a given total output power P_s, the output noise power will be that of a matched amplifier with output noise temperature T.

VII. CONCLUSION

We have presented an analysis of the noise behavior of quasi-optical grid arrays. This analysis should be useful for predicting the noise power and patterns for quasi-optical grids. The approach and many of the derivations are general—they should also be applicable to other types of quasi-optical amplifiers. Although the approach assumes an infinite planar array, similar results could be obtained by considering finite arrays. A more generalized method for calculating the active impedance of each element would be necessary. Nuteson *et al.* [16], [17] have successfully developed such an approach for the analysis of quasi-optical systems.

REFERENCES

[1] M. Kim, E. A. Sovero, J. B. Hacker, M. P. De Lisio, J.-C. Chiao, S.-J. Li, D. R. Gagnon, J. J. Rosenberg, and D. B. Rutledge, "A 100-element HBT grid amplifier," *IEEE Trans. Microwave Theory Tech.,* vol. 41, pp. 1762–1771, Oct. 1993.

[2] M. P. De Lisio, S. W. Duncan, D.-W. Tu, C.-M. Liu, A. Moussessian, J. J. Rosenberg, and D. B. Rutledge, "Modeling and performance of a 100-element pHEMT grid amplifier," *IEEE Trans. Microwave Theory Tech.,* vol. 44, pp. 2136–2144, Dec. 1996.

[3] J. Schoenberg, T. Mader, B. Shaw, and Z. B. Popović, "Quasi-optical antenna array amplifiers," in *IEEE MTT-S Int. Microwave Symp. Dig.,* Orlando, FL, May 1995, pp. 605–608.

[4] J. B. Hacker, M. P. De Lisio, M. Kim, C.-M. Liu, S.-J. Li, S. W. Wedge, and D. B. Rutledge, "A 10-watt X-band grid oscillator," in *IEEE MTT-S Int. Microwave Symp. Dig.,* San Diego, CA, May 1994, pp. 823–826.

[5] H.-C. Chang, X. Cao, U. K. Mishra, and R. A. York, "Phase noise in coupled oscillators: Theory and experiment," *IEEE Trans. Microwave Theory Tech.,* vol. 45, pp. 604–615, May 1997.

[6] P. W. Hannan, "The element-gain paradox for a phased-array antenna," *IEEE Trans. Antennas Propagat.,* vol. AP-12, pp. 423–433, July 1964.

[7] W. K. Kahn, "Ideal efficiency of a radiating element in an infinite array," *IEEE Trans. Antennas Propagat.,* vol. AP-15, pp. 534–538, July 1967.

[8] W. Wasylkiwskyj and W. K. Kahn, "Mutual coupling and element efficiency for infinite linear arrays," *Proc. IEEE,* vol. 56, pp. 1901–1907, Nov. 1968.

[9] D. M. Pozar, "The active element pattern," *IEEE Trans. Antennas Propagat.,* vol. 42, pp. 1176–1178, Aug. 1994.

[10] R. V. Churchill and J. W. Brown, *Complex Variables and Applications.* 5th ed. New York: McGraw-Hill, 1990, pp. 239–255.

[11] Z. B. Popović, R. M. Weikle, M. Kim, and D. B. Rutledge, "A 100-MESFET planar grid oscillator," *IEEE Trans. Microwave Theory Tech.,* vol. 39, pp. 193–200, Mar. 1990.

[12] R. M. Weikle II, "Quasioptical planar grids for microwave and millimeter-wave power combining," Ph.D. dissertation, California Inst. Technol., Pasadena, CA, 1992.

[13] R. F. Harrington, *Time-Harmonic Electromagnetic Fields.* New York: McGraw-Hill, 1961, pp. 152–155.

[14] S. C. Bundy and Z. B. Popović, "A generalized analysis for grid oscillator design," *IEEE Trans. Microwave Theory Tech.,* vol. 42, pp. 2486–2491, Dec. 1994.

[15] M. P. De Lisio, "Hybrid and monolithic active quasioptical grids," Ph.D. dissertation, Dept. Elect. Eng., California Inst. Technol., Pasadena, CA, 1996.

[16] T. W. Nuteson, M. B. Steer, K. Naishadham, J. W. Mink, and J. Harvey, "Electromagnetic modeling of finite grid structures in quasi-optical systems," in *IEEE MTT-S Int. Microwave Symp. Dig.,* San Francisco, CA, June 1996, pp. 1251–1254.

[17] T. W. Nuteson, H.-S. Hwang, M. B. Steer, K. Naishadham, J. Harvey, and J. W. Mink, "Analysis of finite grid structures with lenses in quasi-optical systems," *IEEE Trans. Microwave Theory Tech.,* vol. 45, pp. 666–672, May 1997.

Michael P. De Lisio (S'90–A'95–M'96) was born in Southfield, MI, on July 29, 1968. He received the B.S.E. degree in electrical engineering from the University of Michigan at Ann Arbor, in 1990, the M.S. degree in electrical engineering, and the Ph.D. degree from the California Institute of Technology, Pasadena, in 1991 and 1996, respectively.

In January 1996, he joined the Department of Electrical Engineering, University of Hawaii at Mānoa, as an Assistant Professor. His research interests include high-frequency solid-state devices, microwave and millimeter-wave power combining, and monolithic quasi-optical devices.

Dr. De Lisio is a member of Tau Beta Pi and Eta Kappa Nu.

Robert M. Weikle II (S'90–M'91) was born in Tacoma, WA, in 1963. He received the B.S. degree in electrical engineering and physics from Rice University, Houston, TX, in 1986, and the M.S. and Ph.D. degrees from the California Institute of Technology, Pasadena, in 1987 and 1992, respectively.

From January to December of 1992, he was a Post-Doctoral Research Scientist in the Department of Applied Electron Physics, Chalmers University, Gothenburg, Sweden, where he worked on millimeter-wave HEMT mixers and superconducting hot electron bolometers. In 1993, he joined the faculty at the University of Virginia, Charlottesville, where he is currently an Assistant Professor in the Department of Electrical Engineering. His current research interests include microwave and millimeter-wave solid-state devices, quasi-optical circuits and techniques, and high-frequency receivers and multipliers.

Dr. Weikle is a member of the American Physical Society, International Union of Radio Scientists (Commission D), Phi Beta Kappa, Tau Beta Pi, and Eta Kappa Nu.

David B. Rutledge (S'77–M'77–SM'89–F'93) is Professor of electrical engineering at the California Institute of Technology, Pasadena. His research has involved developing integrated-circuit antennas, imaging arrays, active grids, and software for computer-aided design and measurement. He co-authored the educational microwave computer-aided design package "Puff" with over 12 000 copies distributed worldwide. His group has contributed 200 publications to the technical literature. Five of his students have won Presidential Investigator and Career Awards.

Prof. Rutledge was Distinguished Lecturer for the IEEE Antennas and Propagation Society. He received the Microwave Prize awarded by the IEEE Microwave Theory and Techniques Society, and the Teaching Award of the Associated Students of Caltech.